THE JOURNAL OF PHYSICAL CHEMISTRY Letters

Letter

pubs.acs.org/JPCL

Overcoming Film Quality Issues for Conjugated Polymers Doped with F_4TCNQ by Solution Sequential Processing: Hall Effect, Structural, and Optical Measurements

D. Tyler Scholes,[†] Steven A. Hawks,[‡] Patrick Y. Yee,[†] Hao Wu,[‡] Jeffrey R. Lindemuth,[¶] Sarah H. Tolbert,*[,†,‡,§] and Benjamin J. Schwartz*[,†,§]

[†]Department of Chemistry and Biochemistry and [‡]Department of Materials Science and Engineering, University of California, Los Angeles, Los Angeles, California 90095-1569, United States

[¶]Lake Shore Cryotronics, Westerville, Ohio 43082, United States

[§]California NanoSystems Institute, University of California, Los Angeles, Los Angeles, California 90095, United States

Supporting Information

ABSTRACT: We demonstrate that solution-sequential processing (SqP) can yield heavily doped pristine-quality films when used to infiltrate the molecular dopant 2,3,5,6-tetrafluoro-7,7,8,8-tetracyanoquinodimethane (F_4TCNQ) into pure poly(3-hexylthiophene) (P3HT) polymer layers. Profilometry measurements show that the SqP method produces doped films with essentially the same surface roughness as pristine films, and 2-D grazing-incidence wide-angle X-ray scattering (GIWAXS) confirms that SqP preserves both the size and orientation of the pristine polymer's crystallites. Unlike traditional blend-cast F_4TCNQ/P3HT doped films, our sequentially processed layers have tunable and reproducible conductivities reaching as high as 5.5 S/cm even when measured over macroscopic (>1 cm) distances. The high conductivity and superb film quality allow for meaningful Hall effect measurements, which reveal p-type conduction and carrier concentrations tunable from 10^{16} to 10^{20} cm^{-3} and hole mobilities ranging from ~0.003 to 0.02 $cm^2\ V^{-1}\ s^{-1}$ at room temperature over the doping levels examined.

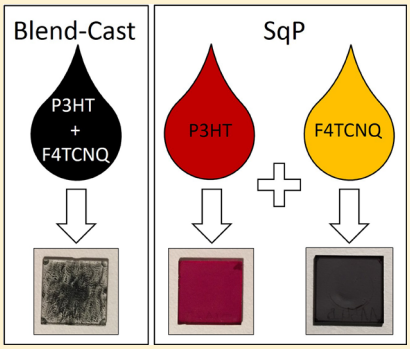

Organic electronics utilize low-cost, solution-processable, and readily tunable semiconducting organic materials in a variety of applications such as LEDs,[1] photovoltaics,[2] thermoelectrics,[3] and transistors.[4] One common way to tune the important electronic properties of this class of materials is through molecular doping, that is, oxidizing or reducing the organic semiconductor to create an appreciable quantity of equilibrium charge carriers.[5−13] Recently, much interest has been focused on the dopant 2,3,5,6-tetrafluoro-7,7,8,8-tetracyanoquinodimethane (F_4TCNQ; see Figure 4a, below, for chemical structure), which has a LUMO level that is deep enough (approximately −5.2 eV relative to vacuum) to oxidize the HOMO of many organic semiconductors.[14] Although there is ample work concerning F_4TCNQ doping of small molecules,[15−20] much of the recent research has focused on the interaction of this dopant with semiconducting polymers.[21−34]

Traditionally, in order to dope conjugated polymers with F_4TCNQ, the two components are combined in solution in the desired dopant/polymer ratio. Due to the favorable energetic offset between the polymer HOMO and the F_4TCNQ LUMO, an electron is readily transferred from the polymer to F_4TCNQ when the two molecules come into contact, leading to charged species that remain closely bound in solution. The high polarity of these species causes them to easily precipitate out of the organic solvents that are used to process the individual materials.[28,35,36] As a result, large highly doped agglomerates form that are not fully solvated, making it difficult to fabricate thin films of sufficient quality to perform meaningful electrical and optical measurements. Raising the temperature of the blended solution can allow for small increases in the solubility of doped polymers in organic solvents;[21,25,28,29] however, high temperatures also have a detrimental effect on doping both in solution[22] and in thin films (see the Supporting Information (SI)). The degree of doping also can be raised slightly without hindering film quality by diluting the doped polymer solution in excess solvent, but this hinders the ability to make films of appreciable thickness by traditional spin-coating methods. Moreover, the neutral F_4TCNQ itself has a limited solubility in most of the organic solvents used to process polymer thin films. This limitation can be partially overcome by synthesizing new, related dopant molecules with increased solubility that can improve polymer/dopant interactions and lead to increased doping density, even with less favorable energetic offsets.[37,38]

Clearly, for molecular doping of semiconducting polymers to be practical, it is important to have a method that affords

Received: October 19, 2015
Accepted: November 10, 2015
Published: November 10, 2015

ACS Publications © 2015 American Chemical Society

DOI: 10.1021/acs.jpclett.5b02332
J. Phys. Chem. Lett. 2015, 6, 4786−4793

tunable (and large) doping concentrations as well as the ability to reproducibly fabricate high-quality films. Here, we show that solution-sequential processing (SqP)[39−43] readily yields films that meet both of these criteria. In SqP, the pure polymer is deposited first from any solvent that produces high-quality films. The molecular dopant is then deposited in a second step from a solvent in which the dopant is soluble and which also swells the polymer film without dissolving it. With the appropriate amount of swelling, molecular dopants can easily infiltrate throughout the polymer film without significantly changing the film's morphology, as our group and others have recently demonstrated for the construction of bulk heterojunction polymer photovoltaics.[43−45] It is important to note that what we call "SqP-based doping" has effectively been applied in the past to doping films of carbon nanotubes,[46−49] doping of polymer films with $NOPF_6$,[12,13] and for patterning conjugated polymer films by taking advantage of the large differential solubility of the doped and undoped regions of the polymer.[50]

In this Letter, we apply the SqP technique to the problem of creating high-quality, heavily doped, highly conductive (>1 S/cm) films of poly(3-hexylthiophene) (P3HT; see Figure 4b, below, for chemical structure) with the molecular dopant F_4TCNQ. We show using optical microscopy, profilometry, and 2-D grazing incidence wide-angle X-ray scattering (GIWAXS) that the SqP technique produces doped P3HT films with a morphology that is nearly identical to that of the original undoped film, save for the incorporation of F_4TCNQ. We perform a side-by-side comparison of doped films produced via the traditional blend-casting method and SqP and show that by changing the concentration of F_4TCNQ and the choice of solvent from which it is cast, we are able to tune the conductivity of P3HT films to virtually any desired level up to 5.5 S/cm. The excellent quality of these doped films allows for this relatively high conductivity to be measured over large distances (>1 cm) and also permits Hall effect measurements to determine the carrier concentration and mobility. Using ultrasensitive AC B-field Hall effect measurements, we find that, for example, a 1.57 S/cm F_4TCNQ SqP doped P3HT film is p-type and has a carrier concentration of $4.3 \pm 0.8 \times 10^{20}$ cm^{-3} with a mobility of 0.024 ± 0.006 cm^2 V^{-1} s^{-1}. With the free-carrier concentration determined, we are also afforded better insight into the UV−visible absorption spectrum of the doped films, and we see the nascent production of equilibrium bipolarons at high dopant concentrations.

We begin our report by first studying the film quality of F_4TCNQ-doped P3HT films produced by the traditional blend-casting method. For the purpose of this study, we maintained the concentration of P3HT in the solvent *o*-dichlorobenzene (ODCB) at 10 mg/mL and added varying amounts of F_4TCNQ to obtain the desired doping ratios, namely, 5, 10, 17, and 30 wt % F_4TCNQ relative to P3HT. We found that the spin-coating conditions that gave the best films were 800 rpm for 60 s, and more details of our sample preparation are given in the SI. The left portion of Figure 1 shows an optical micrograph of a doped blend-cast P3HT thin film. The film is highly nonuniform and made up of large regions of highly doped polymer agglomerates as well as some barren regions that are indicative of poor surface coverage of the blend-doped P3HT by spin-coating. The color difference between the pure, undoped film (right portion of Figure 1) and the doped films results from the doping, which significantly changes the absorption of P3HT, as discussed further below.

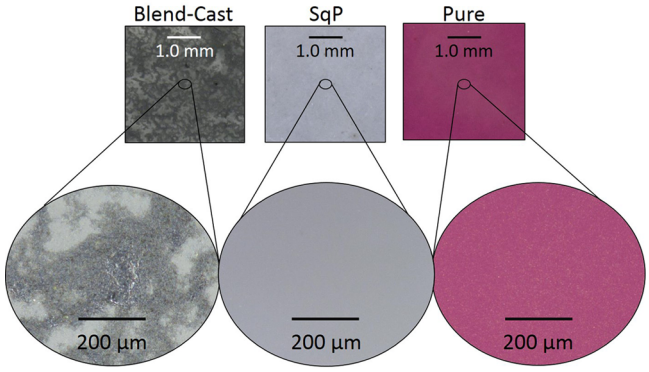

Figure 1. Color optical micrographs at two different length scales of thin films of (left) doped P3HT prepared by the traditional blend-cast doping method with a 30 wt % F_4TCNQ to P3HT doping ratio in ODCB; (center) doped P3HT prepared by the SqP method using 5 mg/mL F_4TCNQ in 75:25 THF/DCM as the casting solvent; and (right) pure, undoped P3HT spun from a 20 mg/mL solution in ODCB for reference.

Figure 2a shows profilometry measurements of the surface roughness of blend-doped P3HT films as a function of the concentration of the F_4TCNQ dopant. The upper portion of Table 1 summarizes the average thickness (d) and root-mean-square (rms) surface roughness (R_{rms}) for these blend-cast films; the roughness continually increases from around 15 nm at 5 wt % F_4TCNQ to >400 nm at 30 wt %. Clearly, traditional

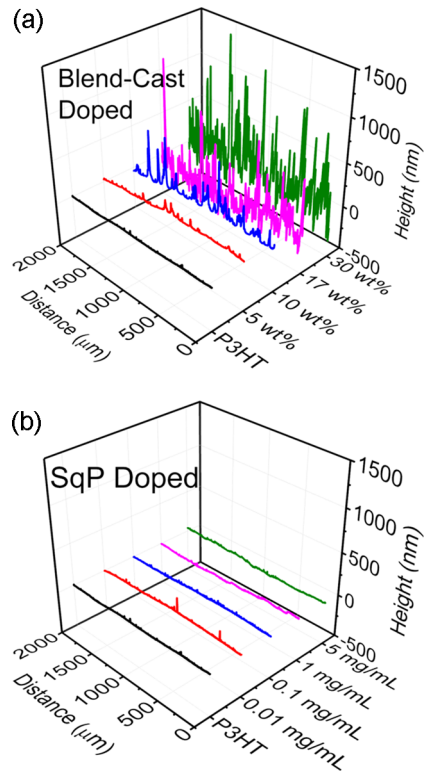

Figure 2. Surface height line scans of doped P3HT films measured by profilometry over a lateral distance of 2 mm prepared by (a) the traditional blend-casting method and (b) the SqP method. A range of dopant concentrations was prepared and measured for both methods. The average thickness and rms surface roughnesses from these scans are summarized in Table 1.

DOI: 10.1021/acs.jpclett.5b02332
J. Phys. Chem. Lett. 2015, 6, 4786−4793

Table 1. Comparison of the rms Surface Roughness (R_{rms}), Film Thickness (d), and Sheet Resistance (R_s) between Different Doping Methods

	R_{rms} (nm)	d (nm)	R_s ($\Omega/\square$)
pure P3HT	4 ± 1	105 ± 5	$>10^8$
Blend Doped			
5 wt %	15 ± 2	56 ± 5	$>10^8$
10 wt %	77 ± 10	120 ± 30	6.5×10^7
17 wt %	220 ± 40	450 ± 100	3.7×10^4
30 wt %	418 ± 200	700 ± 300	2.1×10^4
SqP Doped			
0.01 mg/mL	8 ± 2	110 ± 5	$>10^8$
0.1 mg/mL	8 ± 2	120 ± 12	6.5×10^4
1 mg/mL	11 ± 1	135 ± 5	2.0×10^4
5 mg/mL	8 ± 0.5	135 ± 5	1.5×10^4

blend-casting in the high-doping regime produces films of such poor uniformity that they are unsuitable for device applications or meaningful electrical measurements. The poor film quality of the blend-casting method can be seen by eye (additional images in the SI) and has been noted by others.[35,36,51] As a result, some groups have chosen to study the properties of doped P3HT nanofibers in part to avoid issues with the poor quality of doped blend-cast films.[33,34]

The SqP method, in contrast, allows us to easily overcome all of these issues. The right portion of Figure 1 shows an optical micrograph of a 110 nm thick pristine P3HT film cast from a 20 mg/mL solution in ODCB at 1000 rpm for 60 s. As the corresponding line scans show in Figure 2, such undoped films are quite flat, with a rms surface roughness of only a few nm (Table 1) and no inhomogeneities on optically relevant length scales. When we then dope the film via SqP by spinning a 5 mg/mL solution of F_4TCNQ in a 75:25 tetrahydrofuran (THF)/dichloromethane (DCM) mixture on top of the pure P3HT film at 4000 rpm, the center part of Figure 1 shows that other than the change in film color due to doping, there is essentially no other alteration in the appearance of the film. Indeed, Figure 2b and Table 1 show that the surface roughness of the sequentially processed doped P3HT films stays close to that of the pure P3HT film prior to doping and that the roughness does not increase even as the concentration of the F_4TCNQ solution is increased to the solubility limit.

In addition to the very different macroscopic film structure, we also have explored the molecular-level structural differences between F_4TCNQ-doped P3HT films created via traditional blend-casting and SqP using 2-D GIWAXS. By selectively integrating the 2-D diffraction patterns (as described in the SI), we are able to separate the out-of-plane scattering (corresponding to lattice planes oriented perpendicular to the substrate) and in-plane scattering (corresponding to lattice planes parallel to the substrate). These out-of-plane and in-plane scattering patterns are plotted in Figure 3a and b, respectively, for blend-cast doped P3HT (1 and 17 wt %, orange and red curves, respectively), SqP doped P3HT (1 mg/mL from DCM, blue curves), and undoped P3HT (110 nm thick, green curves). We chose these two blend-cast concentrations because 1 wt % F_4TCNQ is the highest blend concentration that still produces a reasonable quality film and because 17 wt % F_4TCNQ gives approximately the same level of doping as the SqP film, as measured by UV−visible absorption. Because the film thickness and film quality vary drastically across these four samples (see Table 1), we did not thickness-correct the diffraction intensity

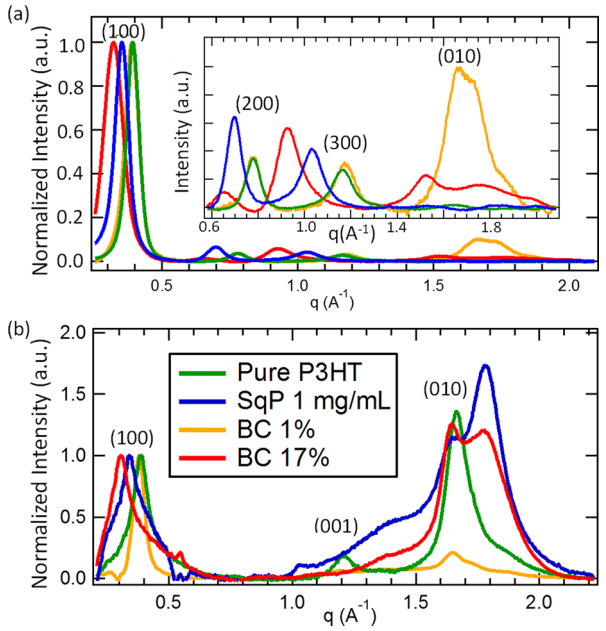

Figure 3. (a) Out-of-plane and (b) In-plane integrated portions of 2-D GIWAXS for films of blend-cast doped P3HT with 1% (orange) and 17% (red) F_4TCNQ by weight, sequentially processed doped P3HT (1 mg/mL, blue curves), and undoped P3HT (110 nm thick, green curves). For better comparison between the films, which have large variations in thickness, the curves are normalized to the height of the (100) peaks. The inset in (a) shows the high-q region on an expanded vertical scale.

but instead normalized all of the diffraction patterns to the height of the (100) diffraction peak. The (100) diffraction peak, which corresponds to the lamellar stacking of the P3HT polymer chains, is centered at 0.39 $Å^{-1}$ in undoped P3HT, corresponding to a lamellar spacing of 16.11 Å. The (010) diffraction peak, which is associated with $\pi-\pi$ stacking, appears at 1.67 $Å^{-1}$ (3.67 Å) in undoped P3HT films.

Although the lamellar diffraction peaks shift to higher d spacing with increasing doping concentration and new peaks appear in the $\pi-\pi$ stacking region, indicating that P3HT cation/F_4TCNQ anion cocrystals form for both SqP doped and blend-cast doped films (as discussed in more detail in the SI),[21,36,51,52] the most interesting comparison between films produced by the two processing techniques is in the crystalline polymer domain orientation. The domain orientation is determined in 2-D GIWAXS by examining the ratio of the out-of-plane to in-plane scattering intensity. For pure P3HT, the high out-of-plane to in-plane ratio seen for the (100) peak and a correspondingly low ratio measured for the (010) peak indicate that the polymer chains are preferentially oriented edge-on to the substrate, as is well-known for P3HT.[53] For the 1 mg/mL sequentially processed doped films, similar diffraction behavior is observed, with the (100) peak appearing most strongly out-of-plane and the (010) peaks appearing almost entirely in-plane. The new $\pi-\pi$ stacking peaks that involve F_4TCNQ in this region at $q \approx 1.4$ and 1.8 $Å^{-1}$ also show the same in-plane orientation. This indicates that despite doping with F_4TCNQ, the sequentially processed doped film maintains P3HT's edge-on molecular orientation with almost no disruption. By contrast, the 1 wt % blend-cast doped film shows significant (010) scattering and scattering from the $q \approx 1.8$ $Å^{-1}$ F_4TCNQ-related peak in both the in-plane and out-of-

DOI: 10.1021/acs.jpclett.5b02332
J. Phys. Chem. Lett. 2015, 6, 4786−4793

plane directions. This suggests that blend-casting alters the P3HT domain orientation, changing it from predominantly edge-on to more isotropic. Presumably, this occurs because in blend-cast doping, solution-phase aggregation plays the dominant role in determining chain orientation in the resultant films.

We note that the scattering from the 17 wt % blend-cast doped film in the $\pi-\pi$ region is more complicated than other samples as the positions of the F_4TCNQ-associated peaks are different in the in-plane and out-of-plane directions. This might arise from substrate orientation, perhaps involving excess F_4TCNQ,[51] or might reflect the fact that edge-on and face-on domains are differently ordered and thus have different $\pi-\pi$ peak positions.[54] Regardless, the presence of significant $\pi-\pi$ scattering intensity in both the in-plane and out-of-plane directions in the 17 wt % doped blend-cast film also suggests that it is much more isotropic than pure P3HT.

It is also worth noting that our 1 mg/mL sequentially processed doped films show a ~15% increase in film thickness after incorporation of F_4TCNQ, as seen in Table 1. This is in reasonable agreement with the 11% increase seen in the lamellar spacing upon doping, suggesting that although there may be a small F_4TCNQ overlayer, the majority of the incorporated F_4TCNQ is intimately integrated into the P3HT lattice. Previous work exploring the use of SqP for polymer-based bulk heterojunction photovoltaics has shown that the swelling of the polymer film by the casting solvent from the second SqP step takes place primarily in the amorphous regions of the film.[44] This is why we believe that the majority of the F_4TCNQ dopant resides in the amorphous regions of our P3HT films. We also believe that the dopant interacts mostly with the surface of the pre-existing P3HT crystallites based on the fact that we see two different P3HT (010) peaks in the doped films. Thus, we expect that the molecular doping is homogeneous from optical length scales at least down to the crystallite size (~10 nm), but we remain unsure as to how much of the dopant actually penetrates into the crystallites and, if so, the dopant's distribution within the crystallites. Despite this uncertainty, all of our data support the idea that the swelling of the P3HT film during SqP allows for efficient intercalation of the F_4TCNQ dopant without significant changes to the P3HT domain orientation and thus the overall film morphology.[44]

Now that we have shown that the SqP method yields F_4TCNQ-doped P3HT films with excellent film quality and relatively unperturbed molecular morphology, we turn next to investigate the electrical properties of these layers. Fortunately, the SqP method allows the degree of doping to be easily tuned simply by altering the concentration of the dopant solution that is cast onto the polymer. We measured the electrical conductivity of a series of films that were doped to different levels via SqP with two different approaches over multiple length scales. The first method was a standard collinear four-point probe measurement with a distance between the probes of 2.5 mm. The second method was the Van der Pauw technique,[55] which used silver paste to make contacts on the corners of 1.5 × 1.5 cm doped films spun onto glass substrates. These measurements yielded values for the conductivity that were in agreement to within 1% of each other despite the large difference in measurement length scales. To further test the scalability of the SqP doping method, we also performed Van der Pauw measurements at the corners of 1 in. square samples. This resulted in measured conductivities that were within 6% of those measured in the smaller samples, demonstrating exemplary scalability.

Figure 4 compares the conductivities of blend-cast doped P3HT films, taken from ref 21, (panel a) with those for the SqP

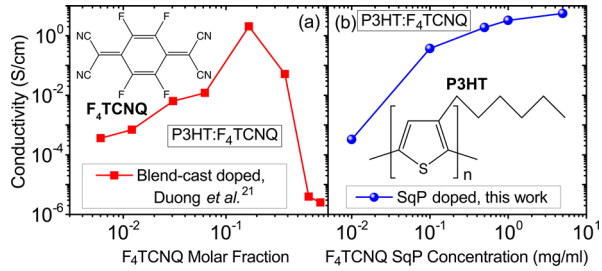

Figure 4. Comparison of the conductivity of P3HT thin films doped with F_4TCNQ by (a) traditional blend-casting method (data taken from ref 21) and (b) our SqP method. The sequentially processed films were prepared by spinning various concentrations of F_4TCNQ onto P3HT films at 4000 rpm. Thicknesses of the different sequentially processed films are given in Table 1. The horizontal axes for the two panels are different because of the differences in processing method; the doping level in (a) is given in units of the mole fraction of F_4TCNQ in the blended solution, while the horizontal axis for (b) is in units of mg/mL F_4TCNQ in the solution used for SqP.

doped films as a function of the concentration of F_4TCNQ in pure DCM (panel b). Although the horizontal axes for the two plots are different, meaning that direct comparison of conductivity at a particular doping level is not possible, the two plots do illustrate the overall trends in conductivity for the two different doping methods with increasing dopant concentration. Figure 4a shows that the amount of F_4TCNQ that can be used to dope P3HT via the blend-casting method is limited as the conductivity (measured over mm distances) peaks near 10 mol % doping and then declines rapidly due to film quality issues.[21] In contrast, Figure 4b shows that the conductivity of the sequentially procesed doped films continues to increase monotonically with increasing dopant concentration to a maximum of 2.7 ± 0.6 S/cm when pure DCM is used as the casting solvent. The conductivity for SqP doped films appears to saturate at the highest dopant solution concentrations, and no decrease is ever observed. The average sheet resistance values that we measured for all of the doped P3HT films are reported in Table 1.

To further increase the amount of F_4TCNQ that intercalates into precast P3HT films, we used a solvent blend that was designed to simultaneously optimize swelling of the P3HT and F_4TCNQ solubility.[44] In this case, we used a 75:25 v/v THF/DCM mixture. We chose THF as the cosolvent because it has much higher F_4TCNQ solubility than DCM, but we were limited to a maximum THF fraction of 75% v/v because any higher fraction of THF led to dissolution of the underlying P3HT films. With this particular solvent blend and a 5 mg/mL F_4TCNQ concentration, we were able to reproducibly fabricate doped P3HT films via SqP with a conductivity averaging 4.5 ± 0.6 S/cm and as high as 5.5 S/cm, which is the highest value reported that we are aware of for a P3HT thin film doped by F_4TCNQ. We also performed experiments where we left the P3HT film to soak in various F_4TCNQ solutions for extended periods of time,[50] but this led to a slight degradation of film quality without achieving either higher doping levels or conductivities. We note that although P3HT has reached higher conductivities when doped with other species such as

DOI: 10.1021/acs.jpclett.5b02332
J. Phys. Chem. Lett. 2015, 6, 4786−4793

Table 2. Summary of Results of the Mean Values of the Hall Voltage (V_H), Hall Coefficient (R_H), Carrier Concentration (p), Resistivity (ρ), and Mobility (μ) from AC B-Field Hall Effect Measurements on SqP Doped P3HT Thin Films with Various Concentrations of F_4TCNQ Casting Solvent

	0.01 mg/mL	0.1 mg/mL	1 mg/mL
V_H (μV)	2.02 ± 1.66	1.51 ± 0.3	15.28 ± 3.45
R_H (cm^3/C)	19.3 ± 15.7	0.014 ± 0.003	0.015 ± 0.004
p (cm^{-3})	(4.3 ± 0.3) × 10^{16}	(2.4 ± 0.1) × 10^{20}	(4.3 ± 0.8) × 10^{20}
σ (S/cm)	(1.70 ± 0.02) × 10^{-4}	0.50 ± 0.01	1.57 ± 0.02
μ (cm^2 V^{-1} s^{-1})	(3.3 ± 2.7) × 10^{-3}	(6.7 ± 1.3) × 10^{-3}	(2.4 ± 0.6) × 10^{-2}

iodine[56] or $FeCl_3$,[57] we hypothesize that our SqP method is already close to the site maximum for doping with F_4TCNQ as the interaction has been shown to saturate at approximately a 1:4 dopant-to-monomer ratio.[24]

The film quality with our SqP doping method is so exceptional that it is possible to detangle the carrier concentration and mobility underlying the conductivity via Hall effect measurements, despite the fact that the authors of ref 30 recently claimed that such measurements would likely never be possible on the F_4TCNQ-doped P3HT system. Due to the low intrinsic carrier mobility of P3HT, we found that an AC magnetic field Hall effect measurement was required to obtain accurate and reliable results (see the SI).[58,59] The results of these sensitive room-temperature measurements are presented in Table 2. Table 2 shows that all of our samples had the expected p-type conductivity with carrier concentrations ranging from 4.3 × 10^{16} to 4.3 × 10^{20} cm^{-3} and mobilities ranging from 3.3 × 10^{-3} to 2.4 × 10^{-2} cm^2 V^{-1} s^{-1} for the doping levels examined. These mobility values are similar to previous findings for electrochemically gate-doped p-type P3HT,[60] which leads us to believe that conduction physics similar to those found in ref 60 also govern our samples. The highest charge carrier concentration of 4.3 × 10^{20} cm^{-3} that we observe corresponds to a doping density of roughly 1 carrier per 10 P3HT monomer units assuming a P3HT density of 1.1 g/cm^3. The fact that all of our samples registered as p-type suggests that there is no significant anomalous Hall effect due to certain types of hopping conduction or inhomogeneous distribution of doping.[5,61−63]

With these considerations in mind and the free-carrier concentration determined experimentally via the Hall effect, we now examine the UV−vis−NIR absorption in order to gain new understanding of the optical properties of F_4TCNQ/P3HT films. We note that the absorption spectrum of blend-doped F_4TCNQ/P3HT films has been explored by several groups,[23,26,30] but a detailed assignment of the various bands and their cross sections has been obscured by the overlap of the anion and polaron spectra and the lack of an independent measurement of the carrier concentration. Using our experimentally determined carrier concentration, we attempted to decompose the absorption spectrum of one of our 1 mg/mL SqP doped films (Figure 5) using the F_4TCNQ solution cross section and previous assignments for the P3HT polaron peaks[30,64] (see the SI for detailed fitting and reference spectrum data). By assuming that the total carrier concentration must be at minimum the value of the free-carrier concentration measured by the Hall effect, then we also must assume this to be the minimum possible anion concentration (because there must be one anion per carrier, and the Hall effect measurement measures only free and not trapped carriers). When using our measured Hall carrier concentration to try to fit the absorption spectrum, however, it quickly became

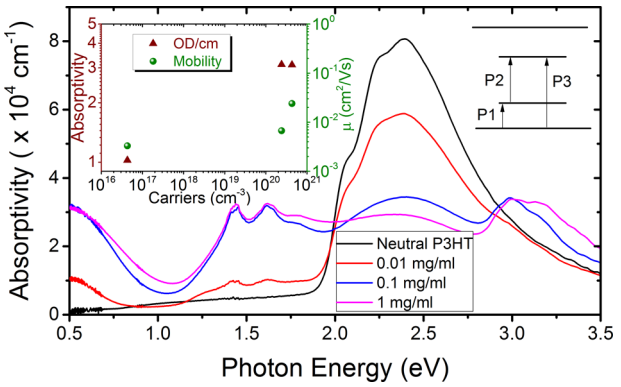

Figure 5. Thickness-normalized absorbance as a function of increasing F_4TCNQ casting concentration for P3HT films doped by the SqP method. The upper right inset shows an energy level diagram of the various polaron transitions, while the upper left inset shows a plot of how the peak absorbance of the P1 transition at 0.5 eV and the mobility change with free-carrier concentration as measured by the AC B-field Hall effect (Table 2).

apparent that multiplying the carrier concentration by the solution cross section for the F_4TCNQ anion led to an absorbance more than twice as large as what we actually measured. Clearly, the actual cross section of the F_4TCNQ anion in the doped film must be quite a bit lower (and have a different spectral shape) than that in solution, so that analyses of doped films using the solution spectrum and cross section are likely subject to significant error.

Since we are unable to completely detangle all of the various overlapping absorption bands in our measured spectrum because we do not know the spectrum and cross section for the anion in the film, we can instead analyze the P1 polaron transition, which peaks near 0.5 eV, as seen in Figure 5, because this spectral region is free from any overlap with the F_4TCNQ anion (see the SI). By tracking the response of this peak with respect to the free-carrier concentration determined by our Hall effect measurement, we are able to obtain a rough idea of the onset of bipolaron production at the highest doping concentrations. The inset of Figure 5 shows that the absorbance of the P1 polaron transition does not continue to increase as the carrier concentration increases when going from the 0.1 mg/mL casting concentration to the 1 mg/mL casting concentration; this is strongly suggestive of bipolaron formation. Indeed, we observe that at around 0.75 eV, there is a noticeable broadening of the P1 band, which is most likely caused by the growth of the bipolaron transition that is located at a slightly higher energy than the P1 polaron transition, in agreement with other recent work.[57] The increased absorption that we see near 3.2 eV corresponds to neutral F_4TCNQ (see the SI). We believe that this can be attributed to a slight overlayer of neutral F_4TCNQ, mentioned previously, that is

DOI: 10.1021/acs.jpclett.5b02332
J. Phys. Chem. Lett. 2015, 6, 4786−4793

present at high dopant concentrations as well as any F_4TCNQ incorporated into the film that did not undergo charge transfer, as has been seen previously for P3HT films doped with F_4TCNQ by blend-casting.[21,30]

The fact that our samples are sufficiently doped to show the beginnings of bipolaron formation also suggests that these samples have enough carriers to have filled all of the available traps. Decomposing the P1 absorption band into free and trapped carrier components is difficult. However, it has been shown previously through both theory and experiment that at low doping levels, a large portion of the generated polarons are trapped due to Coulomb interactions with the dopant anion, and at high doping levels, it becomes easier to generate free carriers due to screening and state-filling effects.[23,65,66] Because of the rapid increase in mobility that we observe between our 0.1 and 1 mg/mL SqP doped samples, we believe that we have exceeded the necessary amount of doping to lower the activation energy of the Coulomb traps, allowing for more efficient free-carrier generation and higher mobility.[66] The fact that the P1 absorptions of these two samples are hardly different while the Hall effect data show a large increase in the number of free carriers is also highly suggestive of liberating formerly trapped carriers in the more highly doped sample, so that at doping concentrations higher than 1 mg/mL, the vast majority of the carriers are free. We also note that the absorption of the neutral, undoped P3HT in the 2.0−2.8 eV range decreases between the 0.1 and 1 mg/mL SqP doped samples, indicating that the total amount of charge transfer is indeed somewhat higher with the higher concentration of dopant. Given that the P1 absorption does not change concomitantly, we can conclude from the data in Table 2 and Figure 5 that in our most highly doped samples, the majority of the carriers are free and there is a reasonably significant number of bipolarons, both of which we believe are directly attributable to the higher film quality of the SqP doping method.

In summary, we have shown that by utilizing the SqP method, we can overcome the issues of solubility and agglomeration at high dopant concentrations associated with blend-casting to easily prepare F_4TCNQ-doped films of P3HT with superior film quality, scalability, and electrical properties. Profilometry measurements show that our SqP doped films have a similar surface roughness to pristine films, and 2-D GIWAXS experiments show that sequentially processed F_4TCNQ incorporates neatly into the P3HT film structure, maintaining the crystalline domain orientation and much of the overall crystallinity. By varying the concentration of F_4TCNQ and choosing the appropriate casting solvent, the conductivity of doped films can be precisely tuned, achieving values for the P3HT/F_4TCNQ system as high as 5.5 S/cm. The film quality and doping levels are high enough to enable Hall effect measurements to detangle the carrier concentration and mobility, which can exceed 4×10^{20} cm^{-3} and 0.02 cm^2 V^{-1} s^{-1}. In future work, we will take advantage of being able to fabricate highly doped films of sufficient electrical, optical, and morphological quality to decouple the effects of polymer crystallinity and the polymer/dopant energy level offset on the efficiency, stability, and electrical properties of doped semiconducting polymers. Overall, the application of SqP to the molecular doping of organic semiconductors provides another step toward the use of conjugated polymers for a wide variety of real-world device applications.

■ ASSOCIATED CONTENT

Supporting Information

The Supporting Information is available free of charge on the ACS Publications website at DOI: 10.1021/acs.jpclett.5b02332.

Additional figures for optical microscopy, GIWAXS, UV−vis, and the Hall effect of blend-cast and SqP F_4TCNQ-doped P3HT films as well as experimental details (PDF)

■ AUTHOR INFORMATION

Corresponding Authors

*E-mail: tolbert@chem.ucla.edu.
*E-mail: schwartz@chem.ucla.edu.

Notes

The authors declare no competing financial interest.

■ ACKNOWLEDGMENTS

The authors thank Matthew Voss, Jagannadha Reddy Challa, and Erik Farr for insightful discussions on the UV−vis−NIR data. This research was supported by the National Science Foundation under Grant Numbers 1112569 and 1510353. S.A.H. acknowledges previous support from the NSF IGERT: Materials Creation Training Program (MCTP), Grant Number DGE-0654431. Use of the Stanford Synchrotron Radiation Lightsource, SLAC National Accelerator Laboratory, is supported by the U.S. Department of Energy, Office of Science, Office of Basic Energy Sciences under Contract No. DE-AC02-76SF00515. The authors also thank Lake Shore Cryotronics for the use of their Lake Shore model 8400 series AC Hall probe system for the Hall effect measurements.

■ REFERENCES

(1) Burroughes, J. H.; Bradley, D. D. C.; Brown, A. R.; Marks, R. N.; Mackay, K.; Friend, R. H.; Burns, P. L.; Holmes, A. B. Light-emitting Diodes Based on Conjugated Polymers. *Nature* **1990**, *347*, 539−541.

(2) Liang, Y.; Yu, L. Development of Semiconducting Polymers for Solar Energy Harvesting. *Polym. Rev.* **2010**, *50*, 454−473.

(3) Chen, Y.; Zhao, Y.; Liang, Z. Solution Processed Organic Thermoelectrics: Towards Flexible Thermoelectric Modules. *Energy Environ. Sci.* **2015**, *8*, 401−422.

(4) Lu, G.; Blakesley, J.; Himmelberger, S.; Pingel, P.; Frisch, J.; Lieberwirth, I.; Salzmann, I.; Oehzelt, M.; Di Pietro, R.; Salleo, A.; et al. Moderate Doping Leads to High Performance of Semiconductor/Insulator Polymer Blend Transistors. *Nat. Commun.* **2013**, *4*, 1588.

(5) Seeger, K.; Gill, W.; Clarke, T.; Street, G. Conductivity and Hall Effect Measurements in Doped Polyacetylene. *Solid State Commun.* **1978**, *28*, 873−878.

(6) Jarrett, C. P.; Friend, R. H.; Brown, A. R.; De Leeuw, D. M. Field Effect Measurements in Doped Conjugated Polymer Films: Assessment of Charge Carrier Mobilities. *J. Appl. Phys.* **1995**, *77*, 6289−6294.

(7) Chiang, C. K.; Fincher, C. R.; Park, Y. W.; Heeger, A. J.; Shirakawa, H.; Louis, E. J.; Gau, S. C.; MacDiarmid, A. G. Electrical Conductivity in Doped Polyacetylene. *Phys. Rev. Lett.* **1977**, *39*, 1098−1101.

(8) Fincher, C. R.; Ozaki, J. M.; Tanaka, M.; Peebles, D.; Lauchlan, L.; Heeger, A. J.; MacDiarmid, A. G. Electronic Structure of Polyacetylene: Optical and Infrared Studies of Undoped Semiconducting (CH)x and Heavily Doped Metallic (CH)x. *Phys. Rev. B: Condens. Matter Mater. Phys.* **1979**, *20*, 1589−1602.

(9) Baughman, R. H.; Brédas, J.; Chance, R. R.; Elsenbaumer, R. L.; Shacklette, L. W. Structural Basis for Semiconducting and Metallic Polymer/Dopant Systems. *Chem. Rev.* **1982**, *82*, 209−222.

DOI: 10.1021/acs.jpclett.5b02332
J. Phys. Chem. Lett. 2015, 6, 4786−4793

(10) Brédas, J.; Street, G. Polarons, Bipolarons, and Solitons in Conducting Polymers. *Acc. Chem. Res.* **1985**, *18*, 309−315.
(11) Kim, Y. H.; Spiegel, D.; Hotta, S.; Heeger, A. J. Photoexcitation and Doping Studies of Poly(3-hexylthienylene). *Phys. Rev. B: Condens. Matter Mater. Phys.* **1988**, *38*, 5490−5495.
(12) Lögdlund, M.; Lazzaroni, R.; Stafström, S.; Salaneck, W. R. Direct Observation of Charge-Induced pi-Electronic Structural Changes in a Conjugated Polymer. *Phys. Rev. Lett.* **1989**, *63*, 1841−1844.
(13) Lazzaroni, R.; Lögdlund, M.; Stafström, S.; Salaneck, W. R.; Brédas, J. L. The Poly-3-hexylthiophene/NOPF6 System: A Photoelectron Spectroscopy Study of Electronic Structural Changes Induced by the Charge Transfer in the Solid State. *J. Chem. Phys.* **1990**, *93*, 4433−4439.
(14) Salzmann, I.; Heimel, G.; Duhm, S.; Oehzelt, M.; Pingel, P.; George, B. M.; Schnegg, A.; Lips, K.; Blum, R. P.; Vollmer, A.; et al. Intermolecular Hybridization Governs Molecular Electrical Doping. *Phys. Rev. Lett.* **2012**, *108*, 1−5.
(15) Maennig, B.; Pfeiffer, M.; Nollau, A.; Zhou, X.; Leo, K.; Simon, P. Controlled P-type Doping of Polycrystalline and Amorphous Organic Layers: Self-Consistent Description of Conductivity and Field-Effect Mobility by a Microscopic Percolation Model. *Phys. Rev. B: Condens. Matter Mater. Phys.* **2001**, *64*, 1−9.
(16) Zhou, X.; Pfeiffer, M.; Blochwitz, J.; Werner, A.; Nollau, A.; Fritz, T.; Leo, K. Very-Low-Operating-Voltage Organic Light-Emitting Diodes Using a P-Doped Amorphous Hole Injection Layer. *Appl. Phys. Lett.* **2001**, *78*, 410−412.
(17) Pfeiffer, M.; Beyer, A.; Fritz, T.; Leo, K.; Pfeiffer, M.; Beyer, A.; Fritz, T.; Leo, K. Controlled Doping of Phthalocyanine Layers by Cosublimation with Acceptor Molecules: A Systematic Seebeck and Conductivity Study. *Appl. Phys. Lett.* **1998**, *73*, 3202−3204.
(18) Blochwitz, J.; Pfeiffer, M.; Fritz, T.; Leo, K.; Blochwitz, J.; Pfeiffer, M.; Fritz, T.; Leo, K. Low Voltage Organic Light Emitting Diodes Featuring Doped Phthalocyanine as Hole Transport Material. *Appl. Phys. Lett.* **1998**, *73*, 729−731.
(19) Gao, W.; Kahn, A. Electrical Doping: the Impact on Interfaces of π-Conjugated Molecular Films. *J. Phys.: Condens. Matter* **2003**, *15*, 52757−52770.
(20) Walzer, K.; Pfeiffer, M.; Leo, K.; Maennig, B. Highly Efficient Organic Devices Based on Electrically Doped Transport Layers. *Chem. Rev.* **2007**, *107*, 1233−1271.
(21) Duong, D. T.; Wang, C.; Antono, E.; Toney, M. F.; Salleo, A. The Chemical and Structural Origin of Efficient P-Type Doping in P3HT. *Org. Electron.* **2013**, *14*, 1330−1336.
(22) Duong, D. T.; Phan, H.; Hanifi, D.; Jo, P. S.; Nguyen, T.-Q.; Salleo, A. Direct Observation of Doping Sites in Temperature-Controlled, P-Doped P3HT Thin Films by Conducting Atomic Force Microscopy. *Adv. Mater.* **2014**, *26*, 6069−6073.
(23) Pingel, P.; Neher, D. Comprehensive Picture of P-Type Doping of P3HT with the Molecular Acceptor F4TCNQ. *Phys. Rev. B: Condens. Matter Mater. Phys.* **2013**, *87*, 115209.
(24) Pingel, P.; Zhu, L.; Park, K. S.; Vogel, J. O.; Janietz, S.; Kim, E. G.; Rabe, J. P.; Brédas, J. L.; Koch, N. Charge-Transfer Localization in Molecularly Doped Thiophene-Based Donor Polymers. *J. Phys. Chem. Lett.* **2010**, *1*, 2037−2041.
(25) Ghani, F.; Opitz, A.; Pingel, P.; Heimel, G.; Salzmann, I.; Frisch, J.; Neher, D.; Tsami, A.; Scherf, U.; Koch, N. Charge Transfer in and Conductivity of Molecularly Doped Thiophene-Based Copolymers. *J. Polym. Sci., Part B: Polym. Phys.* **2015**, *53*, 58−63.
(26) Gao, J.; Niles, E. T.; Grey, J. K. Aggregates Promote Efficient Charge Transfer Doping of Poly(3-hexylthiophene). *J. Phys. Chem. Lett.* **2013**, *4*, 2953−2957.
(27) Glaudell, A. M.; Cochran, J. E.; Patel, S. N.; Chabinyc, M. L. Impact of the Doping Method on Conductivity and Thermopower in Semiconducting Polythiophenes. *Adv. Energy Mater.* **2015**, *5*, 1−8.
(28) Cochran, J. E.; Junk, M. J. N.; Glaudell, A. M.; Miller, P. L.; Cowart, J. S.; Toney, M. F.; Hawker, C. J.; Chmelka, B. F.; Chabinyc, M. L. Molecular Interactions and Ordering in Electrically Doped Polymers: Blends of PBTTT and F4TCNQ. *Macromolecules* **2014**, *47*, 6836−6846.
(29) Aziz, E.; Vollmer, a.; Eisebitt, S.; Eberhardt, W.; Pingel, P.; Neher, D.; Koch, N. Localized Charge Transfer in a Molecularly Doped Conducting Polymer. *Adv. Mater.* **2007**, *19*, 3257−3260.
(30) Wang, C.; Duong, D. T.; Vandewal, K.; Rivnay, J.; Salleo, A. Optical Measurement of Doping Efficiency in Poly(3-hexylthiophene) Solutions and Thin Films. *Phys. Rev. B: Condens. Matter Mater. Phys.* **2015**, *91*, 1−7.
(31) Zhu, L.; Kim, E.-G.; Yi, Y.; Brédas, J.-L. Charge Transfer in Molecular Complexes with 2,3,5,6-Tetrafluoro-7,7,8,8-tetracyanoquinodimethane (F_4TCNQ): A Density Functional Theory Study. *Chem. Mater.* **2011**, *23*, 5149−5159.
(32) Pingel, P.; Schwarzl, R.; Neher, D. Effect of Molecular P-Doping on Hole Density and Mobility in Poly(3-hexylthiophene). *Appl. Phys. Lett.* **2012**, *100*, 143303/1−143303/3.
(33) Gao, J.; Stein, B. W.; Thomas, A. K.; Garcia, J. A.; Yang, J.; Kirk, M. L.; Grey, J. K. Enhanced Charge Transfer Doping Efficiency in J-Aggregate Poly(3-hexylthiophene) Nanofibers. *J. Phys. Chem. C* **2015**, *119*, 16396−16402.
(34) Hu, J.; Clark, K. W.; Hayakawa, R.; Li, A. P.; Wakayama, Y. Enhanced Electrical Conductivity in Poly(3-hexylthiophene)/Fluorinated Tetracyanoquinodimethane Nanowires Grown with a Porous Alumina Template. *Langmuir* **2013**, *29*, 7266−7270.
(35) Deschler, F.; Riedel, D.; Deák, A.; Ecker, B.; von Hauff, E.; Da Como, E. Imaging of Morphological Changes and Phase Segregation in Doped Polymeric Semiconductors. *Synth. Met.* **2015**, *199*, 381−387.
(36) Gao, J.; Roehling, J. D.; Li, Y.; Guo, H.; Moulé, A. J.; Grey, J. K. The Effect of 2,3,5,6-tetrafluoro-7,7,8,8-tetracyanoquinodimethane Charge Transfer Dopants on the Conformation and Aggregation of Poly(3-hexylthiophene). *J. Mater. Chem. C* **2013**, *1*, 5638.
(37) Gao, Z. Q.; Mi, B. X.; Xu, G. Z.; Wan, Y. Q.; Gong, M. L.; Cheah, K. W.; Chen, C. H. An organic p-type dopant with high thermal stability for an organic semiconductor. *Chem. Commun. (Cambridge, U. K.)* **2008**, 117−119.
(38) Li, J.; Zhang, G.; Holm, D. E.; Jacobs, I. E.; Yin, B.; Stroeve, P.; Mascal, M.; Moule, A. J. Introducing Solubility Control for Improved Organic P-Type Dopants. *Chem. Mater.* **2015**, *27*, 5765−5774.
(39) Ayzner, A. L.; Doan, S. C.; Tremolet De Villers, B.; Schwartz, B. J. Ultrafast Studies of Exciton Migration and Polaron Formation in Sequentially Solution-Processed Conjugated Polymer/Fullerene Quasi-Bilayer Photovoltaics. *J. Phys. Chem. Lett.* **2012**, *3*, 2281−2287.
(40) Hawks, S. A.; Aguirre, J. C.; Schelhas, L. T.; Thompson, R. J.; Huber, R. C.; Ferreira, A. S.; Zhang, G.; Herzing, A. A.; Tolbert, S. H.; Schwartz, B. J. Comparing Matched Polymer:Fullerene Solar Cells Made by Solution-Sequential Processing and Traditional Blend Casting: Nanoscale Structure and Device Performance. *J. Phys. Chem. C* **2014**, *118*, 17413−17425.
(41) Lee, K. H.; Schwenn, P. E.; Smith, A. R. G.; Cavaye, H.; Shaw, P. E.; James, M.; Krueger, K. B.; Gentle, I. R.; Meredith, P.; Burn, P. L. Morphology of All-Solution-Processed "Bilayer" Organic Solar Cells. *Adv. Mater.* **2011**, *23*, 766−770.
(42) Wang, D. H.; Moon, J. S.; Seifter, J.; Jo, J.; Park, J. H.; Park, O. O.; Heeger, A. J. Sequential Processing: Control of Nanomorphology in Bulk Heterojunction Solar Cells. *Nano Lett.* **2011**, *11*, 3163−3168.
(43) Zhang, G.; Huber, R. C.; Ferreira, A. S.; Boyd, S. D.; Luscombe, C. K.; Tolbert, S. H.; Schwartz, B. J. Crystallinity Effects in Sequentially Processed and Blend-Cast Bulk-Heterojunction Polymer/Fullerene Photovoltaics. *J. Phys. Chem. C* **2014**, *118*, 18424−18435.
(44) Aguirre, J. C.; Hawks, S. A.; Ferreira, A. S.; Yee, P.; Subramaniyan, S.; Jenekhe, S. A.; Tolbert, S. H.; Schwartz, B. J. Sequential Processing for Organic Photovoltaics: Design Rules for Morphology Control by Tailored Semi-Orthogonal Solvent Blends. *Adv. Energy Mater.* **2015**, *5*, 1−11.
(45) van Franeker, J. J.; Kouijzer, S.; Lou, X.; Turbiez, M.; Wienk, M. M.; Janssen, R. A. J. Depositing Fullerenes in Swollen Polymer Layers via Sequential Processing of Organic Solar Cells. *Adv. Energy Mater.* **2015**, *5*, 1−10.

DOI: 10.1021/acs.jpclett.5b02332
J. Phys. Chem. Lett. 2015, 6, 4786−4793

(46) Takenobu, T.; Kanbara, T.; Akima, N.; Takahashi, T.; Shiraishi, M.; Tsukagoshi, K.; Kataura, H.; Aoyagi, Y.; Iwasa, Y. Control of Carrier Density by a Solution Method in Carbon-Nanotube Devices. *Adv. Mater.* **2005**, *17*, 2430−2434.
(47) Sasaki, Y.; Okimoto, H.; Yoshida, K.; Ono, Y.; Iwasa, Y.; Takenobu, T. Thermally and Environmentally Stable Carrier Doping Using a Solution Method in Carbon Nanotube Films. *Appl. Phys. Express* **2011**, *4*, 085102.
(48) Matsuzaki, S.; Nobusa, Y.; Shimizu, R.; Yanagi, K.; Kataura, H.; Takenobu, T. Continuous Electron Doping of Single-Walled Carbon Nanotube Films Using Inkjet Technique. *Jpn. J. Appl. Phys.* **2012**, *51*, 06FD18/1−06FD18/3.
(49) Hong, C. T.; Lee, W.; Kang, Y. H.; Yoo, Y.; Ryu, J.; Cho, S. Y.; Jang, K.-S. Effective Doping by Spin-Coating and Enhanced Thermoelectric Power Factors in SWCNT/P3HT Hybrid Films. *J. Mater. Chem. A* **2015**, *3*, 12314−12319.
(50) Jacobs, I. E.; Li, J.; Burg, S. L.; Bilsky, D. J.; Rotondo, B. T.; Augustine, M. P.; Stroeve, P.; Moule, A. J. Reversible Optical Control of Conjugated Polymer Solubility with Sub-micrometer Resolution. *ACS Nano* **2015**, *9*, 1905−1912.
(51) Cochran, J. E.; Junk, M. J. N.; Glaudell, A. M.; Miller, P. L.; Cowart, J. S.; Toney, M. F.; Hawker, C. J.; Chmelka, B. F.; Chabinyc, M. L. Molecular Interactions and Ordering in Electrically Doped Polymers: Blends of PBTTT and F_4TCNQ. *Macromolecules* **2014**, *47*, 6836−6846.
(52) Méndez, H.; Heimel, G.; Opitz, A.; Sauer, K.; Barkowski, P.; Oehzelt, M.; Soeda, J.; Okamoto, T.; Takeya, J.; Arlin, J. B.; et al. Doping of Organic Semiconductors: Impact of Dopant Strength and Electronic Coupling. *Angew. Chem.* **2013**, *125*, 7905−7909.
(53) Verploegen, E.; Mondal, R.; Bettinger, C. J.; Sok, S.; Toney, M. F.; Bao, Z. Effects of Thermal Annealing Upon the Morphology of Polymer-Fullerene Blends. *Adv. Funct. Mater.* **2010**, *20*, 3519−3529.
(54) Li, H.; Hwang, Y.-J.; Earmme, T.; Huber, R. C.; Courtright, B. A. E.; O'Brien, C.; Tolbert, S. H.; Jenekhe, S. A. Polymer/Polymer Blend Solar Cells Using Tetraazabenzodifluoranthene Diimide Conjugated Polymers as Electron Acceptors. *Macromolecules* **2015**, *48*, 1759−1766.
(55) *Resistivity and Hall Measurements*. http://www.nist.gov/pml/div683/hall_resistivity.cfm#resistivity (2015).
(56) Ukai, S.; Ito, H.; Marumoto, K.; Kuroda, S. I. Electrical Conduction of Regioregular and Regiorandom Poly(3-hexylthiophene) Doped with Iodine. *J. Phys. Soc. Jpn.* **2005**, *74*, 3314−3319.
(57) Yamamoto, J.; Furukawa, Y. Electronic and Vibrational Spectra of Positive Polarons and Bipolarons in Regioregular Poly(3-hexylthiophene) Doped with Ferric Chloride. *J. Phys. Chem. B* **2015**, *119*, 4788−4794.
(58) Lindemuth, J.; Mizuta, S.-I. Hall Measurements on Low Mobility Materials and High Resistivity Materials. *Proc. SPIE* **2011**, *8110*, 81100I/1−81100I/7.
(59) Lindemuth, J. Variable Temperature Hall Measurements on Low-Mobility Materials. *Proc. SPIE* **2012**, *8470*, 84700G/1−84700G/9.
(60) Wang, S.; Ha, M.; Manno, M.; Daniel Frisbie, C.; Leighton, C. Hopping Transport and the Hall Effect Near the Insulator-Metal Transition in Electrochemically Gated Poly(3-hexylthiophene) Transistors. *Nat. Commun.* **2012**, *3*, 1210.
(61) Emin, D. The Sign of the Hall Effect in Hopping conduction. *Philos. Mag.* **1977**, *35*, 1189−1198.
(62) Fukuhara, T.; Masubuchi, S.; Kazama, S. Hall effect in ClO4-doped polythiophene and poly(3-methylthiophene). *Synth. Met.* **1995**, *69*, 359−360.
(63) Munn, R. W.; Siebrand, W. Sign of the Hall Effect for Hopping Transport in Molecular Crystals. *Phys. Rev. B* **1970**, *2*, 3435−3437.
(64) Brown, P.; Sirringhaus, H.; Harrison, M.; Shkunov, M.; Friend, R. Optical Spectroscopy of Field-Induced Charge in Self-Organized High Mobility Poly(3-hexylthiophene). *Phys. Rev. B: Condens. Matter Mater. Phys.* **2001**, *63*, 1−11.
(65) Arkhipov, V. I.; Heremans, P.; Emelianova, E. V.; Adriaenssens, G. J.; Bässler, H. Charge Carrier Mobility in Doped Semiconducting Polymers. *Appl. Phys. Lett.* **2003**, *82*, 3245.
(66) Arkhipov, V. I.; Emelianova, E. V.; Heremans, P.; Bässler, H. Analytic Model of Carrier Mobility in Doped Disordered Organic Semiconductors. *Phys. Rev. B: Condens. Matter Mater. Phys.* **2005**, *72*, 235202.

DOI: 10.1021/acs.jpclett.5b02332
J. Phys. Chem. Lett. 2015, 6, 4786−4793